Annu. Rev. Earth Planet. Sci. 2005. 33:645–71
doi: 10.1146/annurev.earth.33.092203.122541

First published online as a Review in Advance on February 2, 2005

OROGRAPHIC PRECIPITATION

Gerard H. Roe
Department of Earth and Space Sciences, University of Washington, Seattle, Washington; email: gerard@ess.washington.edu

Key Words rain, snow, mountains, topography, weather

■ **Abstract** The influence of surface orography on patterns of precipitation gives rise to some of the most pronounced climate gradients on Earth, and plays a fundamental role in the interaction between the atmosphere and the rest of the Earth System on a wide variety of time scales. The physical mechanisms involved comprise a rich set of interactions encompassing fluid dynamics, thermodynamics, and micron-scale cloud processes, as well as being dependent on the larger-scale patterns of the atmospheric general circulation. Investigations into orographic precipitation have pursued three parallel tracks of inquiry: observations, theory, and modeling. Significant advances have been made in each over the last few decades, and these are summarized and synthesized here. While many aspects of the basic mechanisms responsible for orographic precipitation have been understood, important issues remain unresolved. The sheer number of contributing processes, together with their convoluted interactions, make the quantitative prediction of precipitation in complex terrain a very hard task. However, while prediction of precipitation amounts for any given event may be difficult, various lines of evidence suggest that the patterns of orgraphic precipitation, even on scales of a few kilometers, are much more robust.

INTRODUCTION

The close association between precipitation and orography must have been evident to the earliest humans. Viewed from a distance, for example, a single large mountain peak can be seen to trigger or divert rain-bearing clouds. Those migrating across mountain passes would have experienced changes in the frequency and intensity of precipitation, and the corresponding abrupt transitions in vegetation and animal life would have suggested that such changes were persistent. A rudimentary understanding of the processes involved appears to date back at least to the ancient Greeks, and was arrived at in part by observing the conditions under which ground fog and mists form and recognizing that atmospheric temperature changes with height. In pondering the origin of springs and rivers around 340 B.C., Aristotle writes in *Meteorologica*:

> "Similarly, the majority of springs are in the neighbourhood of mountains and high places, and there are few sources of water in the plains except rivers.

> For mountains and high places act like a thick sponge overhanging the earth and make the water drip through and run together in small quantities in many places. For they receive the great volume of rain water that falls . . . and they cool the vapor as it rises and condense it again to water."[1]

Research efforts appear to have stalled thereafter, and understanding remained little changed. Expressed by Francis Bacon in 1622:

> "Windes do contract themselves into rain, . . . either being burthened by the burthen itselfe, when the vapours are copious, or by the contrary motions of windes, so they be calme and milde; or by the opposition of mountains and promontories which stop the violence of the windes, and by little and little turn themselves against themselves; or by extreme colds, whereby they are condensed and thickened" (cited in Middleton 1966).

As physics flourished during and after the Renaissance, the mysteries of clouds and precipitation drew the attentions of some of the great scientific luminaries of their times, such as Bacon, Hooke, Liebnitz, Halley, Franklin, Descartes, and Dalton, but efforts were hampered by a hazy understanding of fluid dynamics and a lack of measurements (e.g., Middleton 1966). The British Rainfall Organization was established by G.J. Symons in 1859 to create a systematic observation and classification of precipitation. Data was collated from approximately 1800 rain gauges spread across the British Isles, and the effort included the categorizing of orographic precipitation and its relationship with the prevailing synoptic conditions (e.g., Stow 1875). However, it was not until the early twentieth century, and particularly following World War II (e.g., Bonacina 1945, Douglas & Glasspole 1947), that advances in atmospheric dynamics and thermodynamics, together with more detailed observations of the atmosphere and experiments on cloud physics, began to yield a more complete picture. There has followed a profusion of theories, observations, and models of orographic precipitation, and substantial progress has been made in understanding the mechanisms and processes involved.

The classic picture of orographic precipitation is of a mountain range in the midlatitudes whose axis lies perpendicular to the prevailing wind direction. In the climatological average, the windward flank of the mountain range receives much more precipitation than the leeward flank, resulting in the well-known rain shadow that is reflected in sharp transitions in climate, flora, and fauna across the divide. However, a full accounting of the interactions between orography and precipitation actually encompasses a wide gamut. For example,

- Strong monsoonal circulations impinge on the southern flank of the Himalaya (Cherrapunji in the Khasi hills of India recorded 26.5 m of rain in 1860–1861).

[1]It is ambiguous whether the rising vapor referred to here is outside or inside the mountain!

- Shielded from moisture by two adjacent mountain ranges, many decades can pass between rains in the high central valley of the Atacama desert of Chile (e.g., Miller 1976).
- Steady trade winds over Hawaii lead to 7.5 m of rainfall on the northeast side of the island, but the moist atmospheric layer is confined by a strong temperature inversion (i.e., an increase of temperature with height), and the ~4000 m peaks of Mauna Loa and Mauna Kea receive less than 50 cm year^{-1} (e.g., Carbone et al. 1998).
- On the elevated plateau of Antarctica temperatures are so low that much of the precipitation that does fall (less than 5 cm year^{-1} over much of the interior) comes in the form of clear sky precipitation—fine ice crystals settling out from the atmosphere, known as "diamond dust" (e.g., Bromwich 1988).
- In many regions, vigorous afternoon thunderstorms are triggered in summer months owing to intense solar heating on sun-facing slopes (e.g., Banta 1990).
- After landfall, the torrential rains in hurricanes and typhoons can be dramatically modified by orography (e.g., Geerts et al. 2000, Lin et al. 2002).
- In a single storm, small hills can receive twice the precipitation as nearby areas (e.g., Bergeron 1960, 1961).
- Discrete linear bands of precipitating clouds are sometimes observed over small mountain belts (e.g., Kirshbaum & Durran 2004).

Orographic precipitation is a central part of the interaction between the land surface and the atmosphere. Not only is it important for natural ecosystems and for the management of human water resources but it also has significant ramifications for other physical components of the Earth system. For example, on shorter timescales, natural hazards such as flash floods, landslides, and avalanches are impacted by precipitation intensity in mountainous regions (e.g., Caracena et al. 1979, Caine 1980, Conway & Raymond 1993). During the Pleistocene epoch, the location of, and ice flux within, the great continental-scale ice sheets of the ice ages were controlled in part by patterns of snow accumulation (Sanberg & Oerlemans 1983, Kageyama et al. 1999, Roe & Lindzen 2001, Roe 2002). Finally, over millions of years, patterns of orographic precipitation control patterns of erosion and rock exhumation, ultimately acting to shape the form of the mountain ranges (e.g., Beaumont et al. 1992, Willett 1999, Montgomery et al. 2001, Reiners et al. 2003, Anders et al. 2004a, Roe et al. 2004).

This paper is intended as an introduction and review for a general Earth Scientist. It covers at a broad level the observations, mechanisms, and modeling of orographic precipitation, illustrated with some specific examples. However, the range of phenomena and the scientific literature addressing it are vast, and one paper can only scratch the surface. Excellent reviews at a more complete technical level can be found in Smith (1979), Banta (1990), Houze (1993), Barros &

Lettenmaier (1994a), and Smith (2004). The state of current research in the various fields involved in the study of orographic precipitation is well represented in a 2003 special issue of the *Quarterly Journal of the Royal Meteorological Society* (Volume 129, Issue 588).

SATURATION AND AIR TEMPERATURE

The ability of an air parcel to carry water vapor is of fundamental importance in orographic precipitation. A parcel will become saturated (i.e., its relative humidity reaches 100%) if the partial pressure of the water vapor within it, e, attains a threshold value, e^{sat}. This saturation vapor pressure is a sensitive function of temperature, given by the Clausius-Clapeyron relationship, which to good accuracy can be written as

$$e^{sat}(T) = 6.112 \exp\left(\frac{aT}{b+T}\right), \tag{1}$$

where e^{sat} is measured in millibars, T is the temperature measured in degrees Centigrade, $a = 17.67$, and $b = 243.5^{\circ}$C. This expression is accurate to within 0.3% between $-35^{\circ}\text{C} \leq \text{T} \leq 35^{\circ}$C (e.g., Bolton 1980, Emanuel 1994).

A parcel of unsaturated air that encounters terrain and is forced to ascend will expand adiabatically as the pressure drops and cool, and eventually the vapor it contains will reach saturation. At that point, the saturation-specific humidity (the mass of saturated water vapor per unit mass of the parcel) is (e.g., Wallace & Hobbs 1977)

$$q^{sat}(T, z) = 0.622 \frac{e^{sat}(T)}{p(z)}, \tag{2}$$

where $p(z)$ is atmospheric pressure. So the saturated specific humidity is a function of temperature and pressure only. To get a feel for the scales involved, it is useful to make the approximation that atmospheric temperature varies linearly with height: $T = T_0 + \Gamma z$, where z is height, Γ is the temperature lapse rate (which is negative), and the subscript 0 denotes a variable's value at $z = 0$. If ρ is the density of the air then the mass of water vapor per unit volume in a saturated air parcel can be written approximately as

$$\rho q^{sat}(z) = \rho_0 q_0^{sat} \exp(-z/H_m), \tag{3}$$

where

$$H_m = -\frac{b}{a\Gamma}. \tag{4}$$

H_m is therefore a characteristic e-folding scale height for atmospheric moisture. For typical atmospheric values, H_m is approximately 4 km in the tropics and 2 km at high latitudes. A useful rule of thumb is that a decrease of 10°C halves the saturated moisture content of the atmosphere and that a decrease of 30°C (roughly

the temperature difference between the equator and 60 N or S) reduces it by an order of magnitude. Latitudinal variations consistent with this are clear in observations (e.g., Peixoto & Oort 1992).

Vapor pressures within the atmosphere rarely exceed the saturation value by more than 1% (e.g., Houze 1993), so for a saturated parcel of air ascending with vertical velocity, w, the rate of condensation of water vapor is very close to the rate of change of the saturated moisture content, which can be expressed as

$$C = -\frac{d(\rho q^{sat})}{dt} \simeq -\frac{\partial(\rho q^{sat})}{\partial z}\frac{dz}{dt} = -w\frac{\partial(\rho q^{sat})}{\partial z}. \quad (5)$$

Thus orography influences condensation within the atmosphere by affecting the airflow. The response of the airflow may be stable, or it may be unstable if convection (buoyancy-driven overturning) is triggered. How, and if, the condensation is distributed on the ground as precipitation depends on this atmospheric response, on micron-to-millimeter-scale processes within clouds whereby cloud water is converted to hydrometeors (precipitation particles large enough to fall), and on the ambient humidity of the air through which the precipitation falls, which may cause partial or total reevaporation.

OBSERVATIONS AND MEASUREMENTS

Precipitation Gauges

Figure 1 (see color insert) shows climatological averages from a network of precipitation gauges stretching across the Southern Alps of New Zealand (Wratt et al. 2000). The rain shadow it depicts is one of the most dramatic found anywhere: The Southern Alps are situated squarely in the middle of the midlatitude westerlies at the end of a long fetch over open ocean, and a steady procession of storms impinge on the range. Over the western lowlands 2 to 3 m year^{-1} of precipitation falls. Rates increase sharply over the steep windward slopes, reaching a maximum of 11–12 m year^{-1} at approximately 20 km upwind of the divide. Totals then drop off rapidly to less than 1 m year^{-1} over the eastern plains. The Southern Alps are one of the classic case studies of orographic effects, and the dynamics and mechanisms giving rise to it have been investigated in many papers (e.g., Griffiths & McSaveny 1983; Katzfey 1995a,b; Wratt et al. 1996; Sinclair et al. 1997; McCauley & Sturman 1999; Wratt et al. 2000). Through the asymmetric erosion that it creates, this precipitation pattern has significant consequences for the geological processes acting to create the mountain range (e.g., Willett 1999).

Larger mountain ranges, such as the Southern Alps, typically have maximum precipitation rates occurring away from the crest on the windward flank, although during an individual storm it is possible that the maximum occurs to the lee (e.g., Hobbs et al. 1973, Sinclair et al. 1997). For smaller mountains and hills the maximum is much more likely to be located at or near the crest. The phenomenon of precipitation over small hills was explored in depth by Tor Bergeron. He

established Project Pluvius in 1953, a dense network of approximately 200 rain gauges over an area about 30 km square. The experiment was conducted over a region of Norway where the largest orographic features were ~50 m high, initially chosen deliberately to minimize orographic effects. Much to Bergeron's surprise he found that over these small hills precipitation rates could be twice as high as adjacent areas, and that the differences persisted across different storms. These results led him to write that

> "I venture to state that in no country is the official network of rainfall stations dense enough to give even just a summary picture of the precipitation conditions" (Bergeron 1961).

The density of rain gauge networks has not changed much since, and the problem is particularly acute in mountainous terrain where precipitation gauges are often few and far between. Gauges themselves also suffer from a number of errors, including the disturbance of the local airflow and the undercatch of blowing snow, both of which have systematic elevation biases. Groisman & Legates (1994) estimate biases in climatological measured precipitation rates in the United States of up to 25%, being greatest in high elevations with a lot of snow. Furthermore, precipitation gauges are often sited preferentially in valleys (e.g., Frei & Schär 1998), and because they are only point measurements, any extrapolation to a continuous field must make implicit or explicit assumptions about how orography influences precipitation (e.g., Daly et al. 1994). Caution is needed in using information from precipitation atlases that rely on statistical relationships that may not be generally applicable.

Offsetting these problems somewhat is the fact that gradients in precipitation over orography are often much larger than the amplitude of these errors. The European Alps are perhaps the most densely gauged of any mountain range in the world. Several thousand gauges with an average spacing of 10–15 km allow Frei & Schär (1998) to produce a 20-year climatology at 25-km resolution, although the interpolation is purely statistical. Overall, the basic pattern (Figure 2*b*, see color insert) does not have a well-defined rain shadow: Precipitation maximizes at approximately the same value on the northern and southern flanks, and at rates roughly twice as large as in the higher interior. The Laggo Maggiore region, indicated in the figure, is notorious for intense precipitation events during the autumn that cause widespread flooding and landslides. These storms have been the subject of intense focus in the MAP observing campaign (e.g., Bougeault et al. 2001). The large-scale prevailing atmospheric flow over the Alps in autumn is from almost due west, and so the pattern in Figure 2*b* emphasizes an important point—that prevailing winds and a mountain are, on their own, generally not enough to generate orographic precipitation, and that it usually occurs during the passage of a preexisting weather disturbance (e.g., Smith 2004). In the case of the Alps, intense precipitation on the southern flank occurs when a low-pressure atmospheric trough provides a transient period during the storm when there is strong, moist, and generally southerly flow. The Greenland ice sheet is another place where there is a complex seasonal and

spatial structure to the precipitation pattern because of variable circulation and storminess (e.g., Ohmura & Reeh 1991, Chen et al. 1997). These effects are significant considerations in inferring how patterns of precipitation may have varied in past climates, especially in situations where the orientation of the mountain range with respect to the prevailing wind is complicated, or where the directions of incident storms may have been more variable in alternative climate regimes.

Satellites

Satellites have become a viable alternative to precipitation gauges for constructing a global-scale picture of precipitation patterns, and they are of course essential over the ocean. Various methods have been employed (e.g., Rasmusson & Arkin 1993, Kidder & Vonder Haar 1995, Levizzani et al. 2002), from correlating the amount of high reflective cloud or outgoing longwave radiation with precipitation amounts (e.g., Arkin & Xie 1994), to using passive microwave remote sensing that measures absorption and scattering by precipitation particles (e.g., Chang et al. 1993a,b), to microwave brightness temperatures (e.g., Spencer 1993). Several of these techniques are only useable (or have been properly calibrated) over open ocean. Recently, however, the introduction of new instruments and the reduction in size of the spatial footprint of an individual measurement has allowed satellites to begin to investigate patterns of orographic precipitation. The tropical rainfall measuring mission (TRMM) satellite was launched in 1997 in a low-latitude orbit (36S to 36N) designed to be sun asynchronous, so as to capture the diurnal cycle in precipitation (Simpson et al. 1998, Kummerov et al. 2000). It carries the first space-borne precipitation radar, which has an ovoid spatial footprint of approximately 4 km by 6 km. The instrument measures a profile of radar reflectivity at 80 vertical levels with 250-m spacing, and an iterative algorithm is used to convert the measured reflectivity profile into an estimated true reflectivity profile and finally into a profile of precipitation rate (Iguchi et al. 2000, Kawanishi et al. 2000).

Figure 3 (see color insert) shows the TRMM-derived precipitation pattern compiled for four years (1998 to 2001) over the Himalayas at 10-km resolution (Anders et al. 2004c). Precipitation is largely monsoonal, coming in the months of May through August, although occasional winter storms can be important, especially at high elevations (Lang & Barros 2004). The satellite-derived pattern captures the well-known overall features: wet Indian plains, the dry interior of Tibet, an intense band of precipitation along the southern flank of the Himalayas, and the general drying trend toward the west. It also shows some remarkable smaller-scale structure. A double band stretches along the central portion of the Himalayas and corresponds approximately to the Lesser and Greater Himalaya. In addition, at the scale of the largest valleys and ridges (>30 km), valleys receive much more precipitation than adjacent ridges. Many of these large ridges exceed 4000 m in elevation and so the water vapour content of the overlying atmosphere will be much lower than the neighboring valleys. The pattern measured in the region around Namche Barwa and the spectacular Tsangpo gorge (which together result in

approximately 5 km of vertical relief) is shown in the inset of Figure 3. At smaller spatial scales, however, significant precipitation is observed to reach these high elevations (Barros et al. 2000), presumably though the advection of cloud water and hydrometeors. This scale dependence of the precipitation pattern is an important aspect of orographic precipitation.

Satellite-derived patterns like those shown in Figure 3 need to be very carefully evaluated. One major issue is infrequent observations (about once a day at the latitude of Tibet) because of a low-altitude orbit (∼400 km). Theoretical calculations of this sampling error can be made by making assumptions about the statistical characteristics of precipitation events (e.g., Shin & North 1988, Bell & Kundu 2000). For the observations in Figure 3, these error estimates range between 15% and 60% of the annual precipitation, with a best estimate of 30% (similar to that found by performing Monte Carlo simulations of satellite sampling of gauge data with high temporal resolution). The upper end of this range is certainly large, but even so, it is still smaller than the observed precipitation differences, allowing confidence that the pattern, at least, is meaningful. Furthermore, the precipitation pattern remains essentially the same in each of the four years (even though total amounts differ), and it also does not depend on satellite look angle, suggesting that back-scattering from the irregular surface is not a systematic error (Anders et al. 2004c).

Other issues surround the algorithms translating observed radar reflectivity into near-surface precipitation rate. Such algorithms incorporate information about the freezing level, type of precipitation (stratiform or convective), phase (ice, water, or mixed), and surface clutter (e.g., Kawanishi et al. 2000). However, the standard algorithms have not necessarily been calibrated or optimized for mountainous terrain. Nevertheless, to within the sampling error, TRMM precipitation rates agree with local precipitation gauge measurements, and integrating the pattern over 20 drainage basins of widely varying sizes gives estimated discharge in agreement with observed streamflow data with standard error of 10% to 15% (Anders et al. 2004c). The Global Precipitation Mission (GPM), which will have a similar spatial resolution to TRMM, and which is anticipated to launch in 2012, promises a major new window on patterns of orographic precipitation.

Ground-Based Radar

The use of radar to investigate precipitation dates back to its invention prior to World War II. Various techniques have been developed and refined since then, and radar's ability to provide information about precipitation rates, hydrometeor types, and wind velocities has yielded important insights into the mechanisms of precipitation (see chapter 4 of Houze 1993, and references therein). A transmitted beam of microwave radiation, with wavelengths typically in the range of 1–30 cm, will be scattered by precipitation particles, such that some portion gets backscattered to the receiver and can be analyzed (e.g., Doviak & Zrnić 1984). Three basic parameters can be measured. The first is the the power of the returned signal from

which the reflectivity of the targets can be estimated. For a single particle of diameter D ($D \ll \lambda_{radar}$), Rayleigh theory predicts that the backscattered radiation is proportional to D^6. So for a reflectivity measurement from a given volume of air, and a measured or assumed particle size distribution, the precipitation rate within that volume can be calculated. Reflectivity can also be calibrated directly against rain gauge measurements where available. Complications can arise from the presence of mixed precipitation (i.e., rain and snow), from the attenuation of the radar beam, from the curvature of Earth, and from spurious clutter from objects on the ground (e.g., Houze 1993). The second measure is polarization, which can reveal information about microphysics and can employ either linearly or circularly polarized beams. Oblate falling rain drops produce a different polarization response, for example, than tumbling snowflakes (e.g., Jameson & Johnson 1990, Houze 1993). Large wet snowflakes have a particularly strong effect on polarization, and so the technique can be useful in identifying the melting layer, in which falling snowflakes melt on encountering warmer air. Finally, the Doppler shift in frequency from scattering off of moving targets can be used to calculate the velocity of the hydrometeors in the direction parallel to the radar beam. This velocity combines the terminal fall velocity of the particles relative to the air, and the air velocity itself. Moreover, with two radar beams sited in different locations, an estimate of the terminal fall speed of the hydrometeors, and an assumption of mass continuity, a calculation of the full three-dimensional wind field can be made (e.g., Ray 1990).

National radar networks have broad spatial coverage but tend not to be designed with orographic precipitation in mind. To take full advantage of its capabilities, a radar needs to be carefully located in order that the line of sight of the beam not be blocked by orography, and so use of radar data tends to be restricted to dedicated observing campaigns (during which aircraft can also be used). Browning et al. (1974) and Hill et al. (1981) used ground-based radar to probe the small-scale structure of orographic precipitation over small Welsh hills. They found that precipitation was not steady during storms. The heaviest rates were intermittent and occurred in mescoscale precipitation areas (MPAs) embedded within, and advected by, the large-scale flow. They argued the MPAs resulted from localized regions of convective instability. Other studies also show the precipitation intensity can fluctuate extremely rapidly in time. Figure 4*a* (see color insert) presents a 45-min time series of vertical reflectivity profiles from a storm during the MAP observing campaign in the Alps (from Yuter & Houze 2003). It reveals significant variations on timescales less than 5 min, and reflects the presence of convective or shear-driven turbulence within the airflow. Taking advantage of a well-sited radar, Houze et al. (2001) used radar reflectivity to demonstrate that, even in the climatological average, convection can contribute to the precipitation pattern. In an Alpine transect (shown in Figure 2), Figure 4*b* shows the climatological patterns of radar reflectivity, which are attributable in part to convection. The reflectivity pattern varies on spatial scales of less than 10 km, and were similar in the two years observed.

MECHANISMS OF OROGRAPHIC PRECIPITATION

Cloud Microphysics

Although microphysical processes by definition operate at scales many orders of magnitude less than those typically of interest in orographic precipitation, their effects are of paramount importance in determining how condensation gets distributed over the landscape as precipitation. For example, the terminal fall speed of hydrometeors varies between approximately 1 ms^{-1} for snow and 10 ms^{-1} for heavy rain (and up to 50 ms^{-1} for exceptionally large hail stones). Taking the limits for snow and rain, and a range of horizontal wind speeds from 5 to 30 ms^{-1}, a particle originating at 3 km altitude can get advected anywhere between 1.5 and 90 km before reaching the surface. There are a multitude of possible pathways and interactions for how cloud ice and cloud water particles can grow, combine, and form precipitation. Moreover, their growth and evaporation exchanges latent heat with the surrounding air, which has significant impact on the airflow (e.g., Fraser et al. 1973, Durran & Klemp 1982, Jiang 2003, Steiner et al. 2003). Good introductions to microphysical processes can be found in Wallace & Hobbs (1977) and Houze (1993) for precipitation modeling, and Baker (1997) for general climatic implications, and the references therein.

Clouds form when moisture in the air exceeds its ability to carry water as vapor. Homogeneous nucleation of liquid drops from the vapor phase typically requires supersaturation levels (i.e., e/e^{sat}) of several hundred percent. Because such levels are not observed, almost all condensation must occur though heterogeneous nucleation, in which condensation occurs on aerosol particles called cloud condensation nucleii (CCN). There are also a number of different pathways involved in the formation of ice hydrometeors. Ice particles can be nucleated homogenously (at sufficiently low temperature) or heterogeneously (over a wide range of temperatures) on so-called ice nuclei (IN), or they are formed as a result of certain kinds of collisions of previously existing hydrometeors. The concentration of CCN or IN can affect the number of cloud particles that form and their subsequent evolution. More CCN/IN lead to smaller and more numerous cloud particles for a given condensation rate; fewer CCN/IN and the condensation gets taken up by the smaller number of cloud particles that may grow more rapidly (possibly via a different mechanism), and have faster fall speeds. Hobbs et al. (1973) demonstrated the dramatic potential of this to alter patterns of orographic precipitation over the Casacade range in Washington State. The more IN present, the slower the growth and the slower the fall speed of individual ice hydrometeors, and hence the further the precipitation was advected, in some cases across the divide (Figure 5).

In warm clouds with temperatures above 0°C, cloud droplets grow by the diffusion of water vapor onto the droplets (condensation), or by collisions between droplets to create bigger ones (coalescence). In cold clouds with temperatures below 0°C, supercooled water droplets can in principle coexist with ice particles

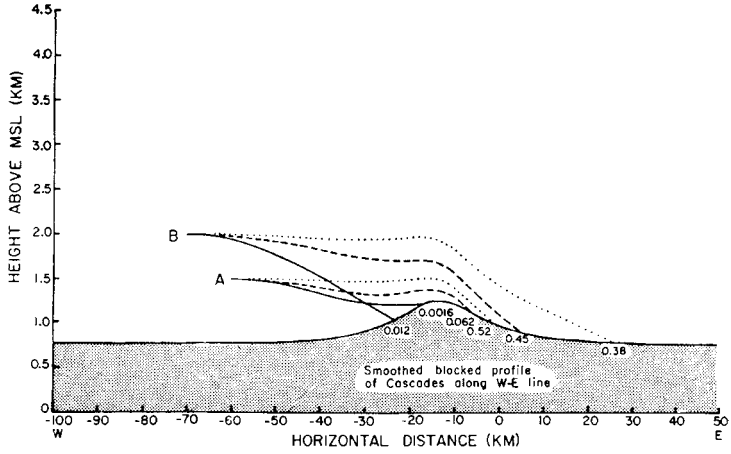

Figure 5 Hydrometeor trajectories from Hobbs et al. (1973) for ice crystals growing by riming in prescribed large-scale flow from left to right. Model follows an initial volume of 1 L from points A and B containing the precipitating ice, and the numbers at the end of each trajectory represent the mass (milligrams) of precipitation that reaches the ground from the original volume. Line types represent different concentrations of crystals as follows: solid, 1 L^{-1}; dashed, 25 L^{-1}; and dotted, 100 L^{-1} (from Banta 1990). Reproduced by permission of the American Meteorological Society.

down to approximately −40°C. Because the saturation vapor pressure over ice is less than that over liquid water at the same temperature, ice particles can grow at the expense of the droplets. Moreover, the freezing of supercooled droplets directly onto ice particles (riming) is a particularly effective mechanism for rapid growth of hail pellets, which, because they have relatively large fall speeds, leads to rapid fallout of cloud water (e.g., Hobbs et al. 1973). In addition, in completely glaciated clouds, ice particles can grow via diffusion of water vapor (deposition) and collision (aggregation).

All of these processes are highly dependent on ambient in-cloud conditions. Thus, the time elapsed between the nucleation of a cloud particle and its incorporation into a falling hydrometeor depends markedly on the situation. In warm cumulus clouds, for example, growth via condensation and coalescence alone can be slow (between 30 and 60 min). On the other hand, condensation accreted onto falling hydrometeors via coalesence, riming, or aggregation reaches the ground comparatively fast. When this growth timescale has been represented explicitly in models of orographic precipitation, studies have suggested values ranging from 100 to 2000 s are necessary to match observations (e.g., Sinclair 1994, Robichaud & Austin 1988, Smith 2003, Smith et al. 2003, Smith & Barstad 2004), which is consistent with the expected theoretical timescales from the various growth processes (e.g., Houze 1993).

Dynamics

The dynamic response of the airflow to the presence of orography as a lower boundary condition sets the three-dimensional pattern of the condensation from which the precipitation results. It also plays an important role in controlling the mechanisms of hydrometeor growth, and their advection and possible evaporation. As already mentioned, the flow cannot be considered independently of the precipitation, the formation and fallout of which is a source of latent heating. Moreover, detailed case studies of individual storms, both observational and numerical, have demonstrated that the flow response can be highly complex (for example, see Rotunno & Ferretti 2001, Medina & Houze 2003, Smith et al. 2003, Steiner et al. 2003 Yuter & Houze 2003, Houze et al. 2001 for the dynamics of orographic precipitation in the Alps alone). Despite this general complexity, various simplified conceptual mechanisms have been proposed against which to evaluate observations or numerical model output. It should be emphasized that during the course of any single event (and certainly in the climatology) more than one mechanism likely operates, but considering them individually can provide a useful basis for thinking about the processes involved.

The most straightforward mechanism of orographic precipitation is stable upslope ascent (Figure 6*a*): Forced mechanical lifting of the air impinging on the windward flank leads to cooling of the air column, resulting in condensation and precipitation; descent in the lee leads to warming and drying, and precipitation is suppressed. At the scale of large midlatitude mountain ranges (perhaps 40 km wide, 1.5 km high) this is certainly a good first-order description (e.g., Smith et al. 2003) of what is going on.

A significant caveat to this picture is that the airflow response must also be a solution to the equations of motion. Parcels of air will always tend to seek their level of neutral buoyancy and so, in a stably stratified atmosphere, forced vertical displacement of the air (such as that created by air crossing from the windward to leeward flanks) creates restoring forces that set up atmospheric gravity waves. These waves may propagate away from the source, or may be trapped and decay exponentially from the surface (e.g., Smith 1979; Durran & Klemp 1982; Durran 1990, 2003), and they are responsible for the lenticular clouds often seen over and downwind of mountain peaks. Examples are shown in Figure 7. In the context of orographic precipitation, these waves mean that ascent can occur ahead of the windward flank of the mountain, and that the vertical extent of the atmosphere that feels the presence of the mountain can be limited. Both of these effects contribute significantly to the region of the atmosphere in which precipitation can be found. Several studies have highlighted how these effects modify the pattern expected from the simple upslope ascent model (e.g., Sarker 1966, Fraser et al. 1973, Smith & Barstad 2004).

If the atmosphere is too stable or the flow is not strong enough, air may be unable to ascend over the range, and at lower levels the flow may become blocked (Figure 6*b*): Flow may get diverted around the mountain or it may stagnate. This

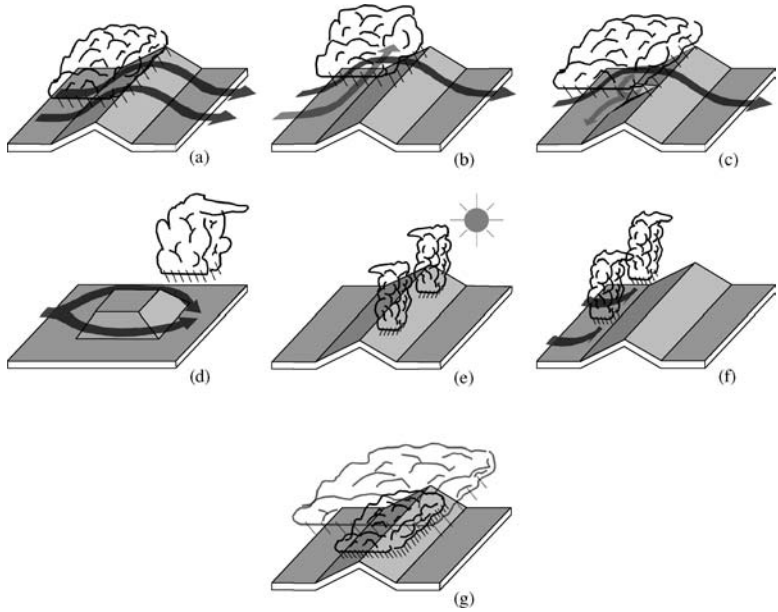

Figure 6 Schematic illustrations of different mechanisms of orographic precipitation. (*a*) stable upslope ascent, (*b*) partial blocking of the impinging air mass, (*c*) down-valley flow induced by evaporative cooling, (*d*) lee-side convergence, (*e*) convection triggered by solar heating, (*f*) convection owing to mechanical lifting above level of free convection, and (*g*) seeder-feeder mechanism. See text for more details.

blocked air can cause ascent further windward of the range and can also enhance the lifting (and hence the precipitation) that does occur. The effects of blocking on orographic precipitation and the conditions under which it occurs have been investigated in many studies (e.g., Katzfey 1995a,b; Sinclair et al. 1997; Rotunno & Ferretti 2001; Houze et al. 2001; Jiang 2003; Medina & Houze 2003). A related effect has been observed in large rain storms in the Alps. Melting and evaporating precipitation cools the air through which it falls, and the result can be strong down-valley air flow (Figure 6*c*). Again, the impinging air mass must rise over this blocking air (Steiner et al. 2003). It has been argued that this contributes to the precipitation pattern (Houze et al. 2001), although it remains to be seen how widespread or significant this interesting mechanism is. Lastly, the diverted airflow itself can lead to precipitation. For example, the Puget Sound region in Washington State often experiences a "convergence zone" when the atmospheric flow, which has split around the relatively narrow Olympic mountains, converges in the lee of the range, where ascent occurs (Figure 6*d*; Mass 1981).

Another notable part of the atmospheric response to orography is the possible triggering of unstable convection (e.g., Banta 1990). If the orography lifts air

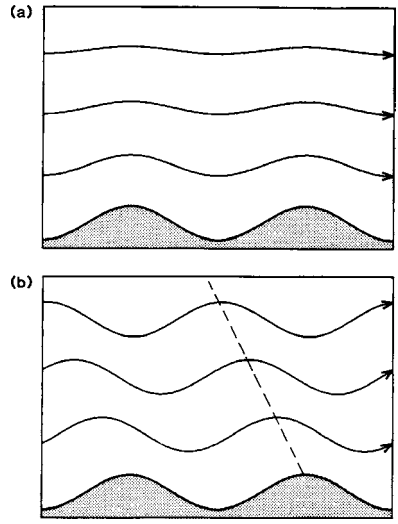

Figure 7 Examples of atmospheric gravity waves. Streamlines in steady, left-to-right airflow over an infinite series of sinusoidal ridges examples representing (*a*) a narrow ridge case, with waves decaying exponentially with height, and (*b*) a broad ridge case, with waves propagating vertically. The dashed line in (*b*) shows the upstream phase tilt of lines of constant phase (after Durran 1990). See Durran (1990, 2003) for details.

above its level of free convection (the level at which it becomes less dense than its surroundings) it will continue to rise (Figure 6*e*). This unstable ascent not only enhances the condensation rate locally, but also can produce greater amounts of super-cooled cloud water droplets, leading to riming onto ice particles, and hence the efficient fall-out of precipitation particles that would otherwise grow more slowly. Convecting cells of air may be embedded within stratiform clouds owing to larger scale ascent, or may occur in isolation. Another trigger of orographic convection is solar heating on sun-facing slopes, which is responsible for the afternoon thunderstorms in summer that occur in many mountainous regions (Figure 6*f*).

A final mechanism that is commonly invoked is the "seeder-feeder" mechanism (Bergeron 1950, 1968). It was proposed to explain the amplification of precipitation over hills that were too small to generate precipitation themselves because air traverses them too quickly for hydrometeors to form by condensation and coalescence alone. The mechanism is invoked in the literature in a variety of situations, and in ways that can occasionally be confusing. Sometimes it is envisioned that there is a large-scale precipitating cloud (the "seeder") at high levels that is essentially undisturbed by the orography below, and a cap cloud (the "feeder") caused by low level ascent over the hill (Figure 6*g*). Falling precipitation from the seeder cloud accretes additional moisture when it falls through the feeder cloud, either by coalesence or by riming, and so precipitation is enhanced over the hill (e.g., Bader

& Roach 1977, Hill et al. 1981, Robichaud & Austin 1988). At the other extreme of its usage, a deep orographically triggered convective cloud can be described as having a seeder region (i.e., falling rimed particles) and a feeder region of cloud water (i.e., low-level warm sector of the cloud) (e.g., Browning et al. 1974, Hobbs et al. 1980, Sinclair 1994). Wash-out of cloud water by falling hydrometeors is undoubtedly an important process in orographic precipitation, but it can arise from a variety of different circumstances. Thus, there is not a clear distinction between upslope ascent and seeder-feeder, and the differences are perhaps somewhat semantic. The common theme of these mechanisms is that orographically induced ascent produces a condensation region. How and if that condensation reaches the ground as precipitation depends on the dominant conversion mechanisms operating at the time.

MODELING OF OROGRAPHIC PRECIPITATION

Diagnostic Models

A useful quantitative benchmark against which to evaluate orographic precipitation rates is the total condensation rate in a vertical column of a saturated atmosphere, where at every level the vertical velocity equals the orographically forced lifting at the surface (e.g., Sawyer 1956, Smith 1979). This measure is a sensible upper bound on the precipitation rate that can be achieved owing to stable upslope ascent of saturated air. If $w = \vec{u} \cdot \nabla z_s$, where z_s and u are the surface elevation and wind speed, respectively, then from Equation 5, this condensation rate, S, is given by

$$S = -\int_{z_s}^{\infty} \vec{u} \cdot \nabla z_s \frac{d}{dz}[\rho q^{sat}]\, dz$$

$$= \rho_0 q_0^{sat} \vec{u} \cdot \nabla z_s e^{-\frac{z_s}{H_m}}. \quad (6)$$

For typical midlatitude values ($|\vec{u}| \simeq 10$ ms^{-1}, $\nabla z_s \simeq 2/50$, $\rho_0 \simeq 1.2$ kgm^{-3}, and $q_0^{sat} = 8$ gkg^{-1}), and surface wind normal to the local slope, Equation 6 gives $S = 14$ mmh^{-1} at $z_s = 0$, which would be very heavy precipitation. The ratio of the measured precipitation to S can be defined as a precipitation efficiency (e.g., Smith 1979), and is often used as a measure of the effectiveness with which moisture is removed from the atmosphere by orography.

Note that in this basic model, the generation of condensation decreases exponentially with surface height. This is an important effect for larger mountain ranges where elevations are comparable to the moisture scale height (between 2 to 4 km depending on latitude and season), and it is a big part of the reason why, for such ranges, precipitation rates tend to maximize down on the windward slopes.

The simplest models of orogaphic precipitation use equations that are similar to Equation 6 (e.g., Sawyer 1956, Smith 1979, Sanberg & Oerlemans 1983, Alpert 1986). Such models incorporate the basic physics that orographic precipitation

tends to increase with the steeper windward slopes owing to enhanced lifting and tends to decrease with elevation owing to the Clausius-Clapeyron effect. However, it is commonly found in these models that some downwind smoothing of the condensation rate needs to be applied to get precipitation rates consistent with observations and to get any leeside precipitation. It is argued that this smoothing reflects the growth and downwind advection of hydrometeors. For modeling climatological rates of precipitation, a probability distribution of storminess can also be included, which allows for some leeside precipitation to occur (e.g., Roe & Lindzen 2001). Given their simplicity, however, these models are best thought of as providing physically based and calibrated rules for precipitation, rather than being direct parametrizations of a particular physical process.

Another set of quasi-analytical models aim to solve for the air flow in a more realistic way [e.g., Myers 1962 (but see Smith 1979), Sarker 1966, Fraser et al. 1973]. In this class, Smith & Barstad (2004) present a highly adaptable orographic precipitation model incorporating a linear atmospheric response and capable of efficient calculation over complex terrain. Cloud microphysics are represented in their model by characteristic delay timescales for hydrometeor growth and fallout. Other, similar models focus on the seeder-feeder mechanism and parameterize the wash-out of droplets (or ice) from the orographic cloud given an imposed large-scale precipitation rate. (e.g., Bader & Roach 1977, Carruthers & Choularton 1983, Choularton & Perry 1986, Robichaud & Austin 1988). A final set in this category are numerical models that, to varying degrees of complexity, solve for the topographically modified atmospheric flow from the large-scale circulation and include formulations of precipitation formation (e.g., Colton 1976, Rhea 1978, Sinclair 1994, Barros & Lettenmaier 1993). The treatment of microphysics in these models range from including representative (and tuneable) timescales, to an explicit representation of particular growth processes.

The above models are all diagnostic in the sense that for given large-scale atmospheric conditions (i.e., wind and temperatues) the atmospheric flow is calculated, and the amplitude and patterns of the precipitation rates are then diagnosed from that flow assuming a steady state. As such, they are inherently unable to reflect the complexity of the observed transient interactions, which can involve processes like convection, blocking, and valley circulations.

Data are hard to come by in mountainous terrains, therefore models are often evaluated (or more typically calibrated) for a limited data set, sometimes for a particular storm and sometimes for the climatological distribution. With an appropriate optimization of parameters these models are generally able to achieve a good match with observed precipitation rates at the scale of tens of kilometers, which suggests that they do capture many of the important processes involved. However, model skill can vary wildly between different storms, and the same model applied to a different mountain range can perform poorly (e.g., Barros & Lettenmaier 1994a). The implication is that the subtler interactions that make individual storms and locations different from each other are not well handled. This is not particularly surprising. For example, parameterizations of hydrometeor

growth times that have been optimized for a winter storm should not be expected to do well in summer when the dominant microphysical processes have changed. Indeed, Barros & Lettenmaier (1994a) argue for the necessity of a range-by-range calibration of any reduced precipitation model, asserting that the myriad factors controlling precipitation formation make the prevailing synoptic and microphysical conditions for each mountain range essentially unique. A possible way forward is to categorize precipitation events by the combination of orographic and synoptic conditions that give rise to a particular precipitation pattern (e.g., Roe & Baker 2004).

Prognostic Models

With advances in computational power, prognostic numerical models have become a major research tool for the study of orographic precipitation (e.g., Bruintjes et al. 1994; Katzfey 1995a,b; Chen & Huang 1999; Colle et al. 1999; Ferretti et al. 2000; Rotunno & Ferretti 2001; Smith et al. 2003; Colle 2004; Kirshbaum & Durran 2004; Lang & Barros 2004). These mesoscale (i.e., ∼100 to 1000 km) models integrate the full dynamical equations of motion forward in time and can be run at horizontal resolutions at which individual convecting (i.e., cloud-like) elements can be resolved (∼1 km), and with tens of layers in the vertical. In addition to the dynamics, there is also the model "physics" (e.g., Grell et al. 1995): Models can incorporate sophisticated moisture and precipitation schemes in which many different categories of cloud and precipitation particle types, and the mechanisms that exchange mass between them, are explicitly represented (e.g., Houze 1993), and which interact fully with the atmospheric flow. Typically, they also include comprehensive representations of radiative processes and atmosphere-land surface interactions. Lastly, such models must be supplied with lateral boundary conditions. For simulations of actual storms, this means using global-scale atmospheric data sets, such as the reanalysis products available from the National Center for Environmental Prediction–National Center for Atmospheric Research (NCEP-NCAR; Kalnay et al. 1996) or the European Center for Medium Range Forecasting (ECMWF; Simmons & Gibson 2000). For past or future simulations, output from global climate models (GCMs) can be used. More idealized boundary conditions may also be specified for process-oriented studies.

Mesoscale models can thus be configured in a dizzying variety of ways. For given computational resources, significant trade-offs must be made between things like the area covered by the model domain, the horizontal and vertical resolution of the model, the length and number of different integrations desired, and complexity of the model physics included. Although the output from such complicated models can be daunting to understand, they have the potential to investigate the full range of precipitation-producing mechanisms. Well-designed numerical experiments can isolate the sensitivity of precipitation rates to particular processes, and the output can also be used to evaluate the simpler conceptual pictures. For example, Smith et al. (2003) simulated one Alpine storm and found that far from a

smooth descent after crossing the range crest as envisioned in the classic upslope precipitation model, individual air parcels actually experienced a wide variety of heating and cooling histories, and that consequently the air mass became surprisingly scrambled over the leeward flank.

Owing to the computational constraints, the use of mesoscale models to investigate orographic precipitation has generally been limited to case-studies of one, or at most a few, storms. In some places, however, mesoscale models are routinely used for making weather forecasts. At the University of Washington, the Penn State/NCAR MM5 mesoscale model (Grell et al. 1995) has been run operationally at 4-km resolution over the Pacific Northwest for the past six years (e.g., Colle et al. 1999). The climatological precipitation pattern from the model output shows a clear association with the topography (Figure 8*b*,*c*, see color insert): Windward ridges receive approximately twice as much precipitation as the adjacent valleys. This pattern occurs in both 2000 and 2001 despite the annual totals differing by approximately 40%. Although which ridge receives the most precipitation varies, the same basic pattern is seen in almost all storms with appreciable precipitation, and across all seasons (Figure 8*d–i*). It is important to stress that the prevailing wind strength and direction differs between storms, and it also varies during each individual storm as the synoptic conditions evolve. However, the maximum precipitation rates generally occur during the period of the storm when strong moist airflow is most nearly oriented up the mountain slopes. A closely spaced network of precipitation gauges was installed on a transect across one of the major ridges (shown as a line in Figure 8*a*) during the October 2003 to May 2004 rainy season to evaluate the MM5 model performance in capturing this pattern (Anders et al. 2004c). The observations along this transect for one storm occurring on October 20–21, 2003, are shown in Figure 9, together with the output from an MM5 integration at 4/3 km covering the same period. The model output underestimates this storm total by approximately a factor of two (but see Colle et al. 1999). However, the model gets the ratio of precipitation on the ridge to that in the adjacent valleys consistent with the observations. The observations show that about the same ratio applies in the seasonal average too, lending confidence that the modeled pattern reflects the real situation over the Olympics (Anders et al. 2004b). Simple diagnostic models have some success in reproducing this precipitation pattern (e.g., Barros & Lettenmaier 1993, Smith & Barstad 2004, Anders et al. 2004b). It is consistent with the greatest condensation occurring over low (i.e., moist), steep, windward slopes, plus some downwind advection owing to conversion processes and fallout.

Large-Scale Atmospheric Circulation

Sawyer (1956) separated the factors influencing orographic precipitation into (*a*) cloud processes, (*b*) the interaction of the atmospheric flow with orography, and (*c*) the larger-scale atmospheric circulation. This remains a useful classification. Climatological rates of orographic precipitation depend on the frequency and intensity of storms, which in turn are controlled by the larger-scale patterns of

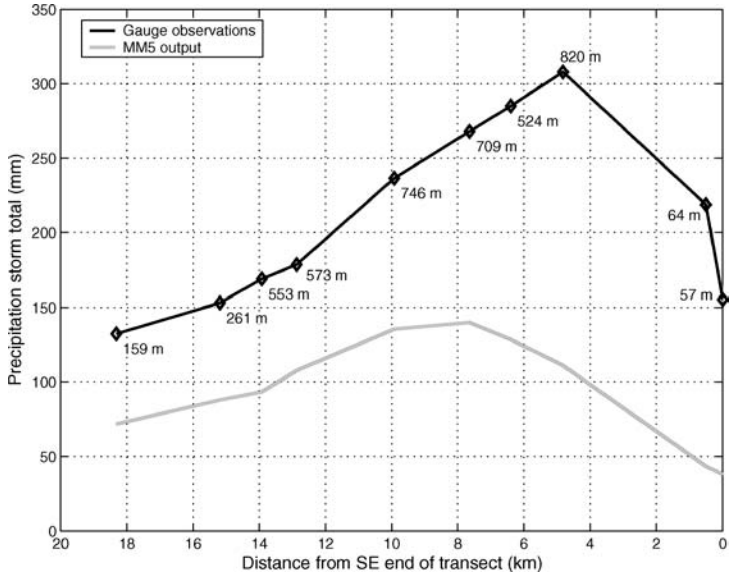

Figure 9 Black diamonds show observations from a network of precipitation gauges located along the transect shown in Figure 8*a*, for one storm October 20–21, 2003. The elevation of the gauges are noted by each point. The grey line is the output from an MM5 integration run at 4.3 km for the same storm.

the general circulation. It is well understood in the modern climate how, for example, the El Niño Southern Oscillation (ENSO), the Arctic Oscillation (AO), and interannual variability in the Indian monsoon lead to changes in storminess and precipitation (e.g., Dai & Wigley 2000, Thompson & Wallace 2001, Krishnamurthy & Shukla 2000). On longer timescales, paleoclimate proxies have been used to infer significant variability in circulation patterns in the AO (e.g., Noren et al. 2002), ENSO (e.g., Koutavas et al. 2002), and the Indian and Asian monsoons (An et al. 2001, Wang et al. 2001). Direct paleoclimate records of orographic precipitation exist in the accumulation rates stored in ice sheets and mountain ice caps (e.g., Kapsner et al. 1995, Rupper et al. 2004). However, the relationships between atmospheric circulation patterns and local orographic precipitation are not necessarily constant over time and need to be carefully assessed. Unfortunately, storminess and precipitation on a regional scale are aspects of the climate that GCMs generally simulate poorly (e.g., IPCC 2001). There is therefore relatively low confidence in model predictions for past and future climates. As an example, it is often assumed that a glacial climate, with a larger pole-to-equator temperature difference, results in a stronger jet stream and a more unstable and stormier atmosphere. In fact, the relationship between wind strength, storminess, and precipitation is not at all straightforward. For instance, a robust characteristic feature of a colder atmosphere is reduced moisture availability. So more frequent or

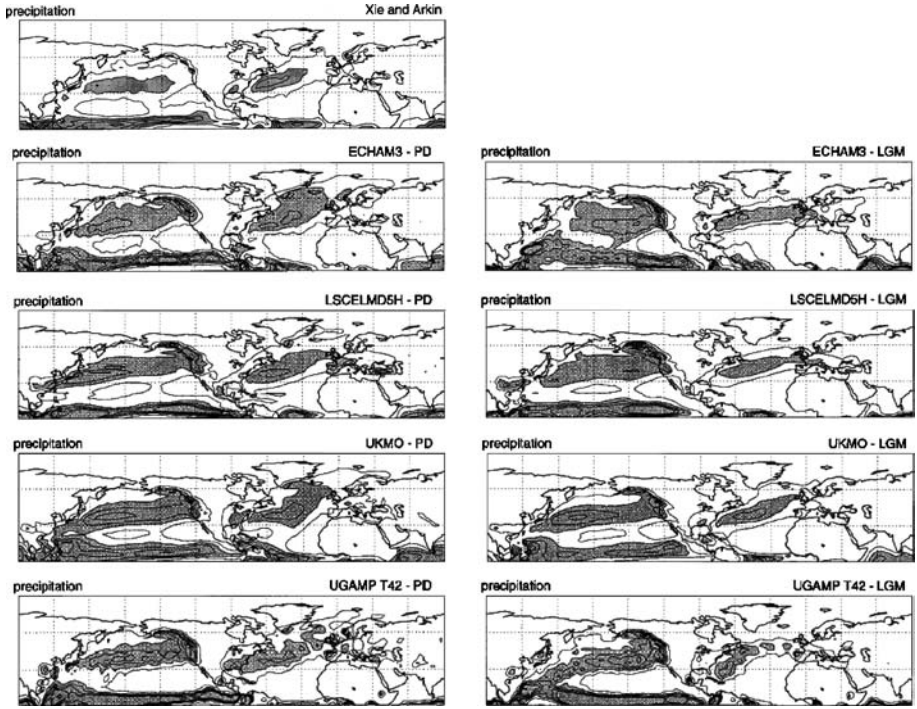

Figure 10 Northern hemisphere wintertime (December, January, and February) precipitation from observations (*top panel*, Xie & Arkin 1997), and for simulations from four different GCMs. The left panels show model results for the present day (PD), the right panels give results for the last glacial maximum (LGM) 21,000 years ago. Precipitation rate contours for 2, 4, 6, 8, and 10 mm day^{-1}, with shading above 4 mm day^{-1}. There are large variations between models in both the LGM and PD simulations, and for many regions, there is no consensus among models about even the sign of the change between PD and LGM. Adapted from Kageyama et al. (1999). Reproduced by permission of the American Meteorological Society.

larger storms do not necessarily carry with them greater precipitation. To illustrate the typical variations between models, Figure 10 shows a selection of results from Kageyama et al. (1999) for GCM simulations of wintertime northern hemisphere precipitation patterns for the current climate and the last glacial maximum (21,000 years ago).

CONCLUSIONS

The existence of a rain shadow across a mountain range whose axis lies perpendicular to the prevailing winds is one of the most confident expectations in atmospheric science. For large mountain ranges, precipitation maximizes over the

windward slopes, whereas for smaller hills the maximum tends to occur nearer the crest. However, the amplitude of the rain shadow and the relationship between orography and precipitation at smaller spatial scales are much more complex questions, and the subject of active research. This review has touched on some of the evidence and scientific issues involved.

At spatial scales greater than approximately 40 km, and for mountain ranges exceeding approximately 1.5 km in height, the forced upslope ascent model generally gives a good basic description of the precipitation pattern. Maximum condensation is generated over low, steep, windward slopes, and the precipitation pattern is offset downwind somewhat, owing to the advection of hydrometeors during their formation and fallout. However, there is now also plenty of evidence of a close association between orography and precipitation patterns at spatial scales of a few kilometers, even in climatological precipitation rates. Observational and modeling studies have suggested various physical mechanisms operate, but it is yet to be determined if one will emerge as dominantly responsible for setting the pattern on these smaller spatial scales. It is more likely that over individual ranges, in particular climate settings, and in particular seasons, the explanations will be different. In that case, the importance of applications (including the prediction and mitigation of natural hazards) will determine where research efforts get focused.

Orographic precipitation is intrinsically a transient phenomenon. It tends to occur during the passage of a preexisting weather disturbance, and precipitation rates can vary substantially during the course of a single storm as synoptic conditions change, as happens, for example, with the passage of a front. Moreover, dynamical effects such as blocking, convective instability, and evaporative cooling may only occur for a fraction of the storm's duration, but can nonetheless make an important contribution to the storm-averaged pattern. Despite the transient nature of orographic precipitation, steady-state diagnostic models have some success in capturing storm-averaged and climatological patterns. One must be careful though about the sense in which the "average pattern" actually exists, and, in calibrating a physical model to emulate that pattern, what the model parameters really reflect. It is inevitable those parameters will, to some degree, be playing a role beyond their nominal physical interpretation.

Much of the research to date on orographic precipitation has focused on storms impinging on midlatitude mountain ranges, and this review has reflected that bias. An important area for future research is to extend investigations in polar and subtropical climates (e.g., Bromwich 1988, Evans et al. 2003, Lang & Barros 2002), which may well prompt new ideas and theories. Another understudied aspect of orographic precipitation is the mechanisms that control patterns of precipitation on the leeward side of mountain ranges. Such patterns can be just as striking as those on the windward flank. For instance, the pronounced dry slot that is apparent in Figure 8*b*,*c* occurs over the Elwha valley in the lee of Mt. Olympus. Although there are no direct precipitation measurements, its vegetation is consistent with a drier climate than the neighboring areas.

Knowledge of precipitation rates in the mountainous terrain of Earth remains sketchy. The advent of global satellite coverage at high resolution, together with

further intensive field campaigns, will help to continue to fill out the picture. It is also clearly of interest to predict orographic precipitation in past and future climates. Given the numerous physical processes involved and their attendant uncertainties, it is perhaps likely that confidence in any particular model prediction will always remain low. A productive approach instead may be to bound the range of changes that are possible in different climates. Understanding the probability distribution of orographic precipitation events in the current climate, as well as the mechanisms responsible, will be useful in evaluating how changes in that probability distribution would lead to different precipitation rates. Furthermore, a variety of indications presented here suggest that while changes in the climatological rates are quite uncertain, patterns of orographic precipitation may be much more robust. Further progress will be made by closely combining new insights from theoretical studies, numerical modeling, and observations.

ACKNOWLEDGMENTS

I am very grateful to Harvey Greenberg for making many of the figures. I also thank Alison Anders for providing the Tibet and Olympics data and MM5 model output; Marcia Baker, Dale Durran, and Richard Lindzen for valuable suggestions on an earlier draft; David Montgomery for guidance to historical references; and Ana Barros and Ron Smith for insightful and instructive conversations about orographic precipitation.

The *Annual Review of Earth and Planetary Science* is online at http://earth.annualreviews.org

LITERATURE CITED

Alpert P. 1986. Mesoscale indexing of the distribution of orographic precipitation over high mountains. *J. Clim. Appl. Meteorol.* 25: 532–45

An Z-S, Kutzbach JE, Prell WL, Porter SC. 2001. Evolution of Asian monsoons and phased uplift of the Himalaya-Tibet plateau since late Miocene times. *Nature* 411:62–66

Anders AM, Roe GH, Durran DR. 2004a. Conference notebook: Orographic precipitation and the form of mountain ranges. *Bull. Am. Meteorol. Soc*. 85:498–99

Anders AM, Roe GH, Durran DR. 2004b. *Orographic precipitation and the form of mountain ranges*. Presented at 11th Conf. Mountain Meteorol., 21–25 June, Mt. Washington Valley, NH

Anders AM, Roe GH, Hallet B, Montgomery DR, Finnegan NJ, Putkonen J. 2004c. Spatial patterns of precipitation and topography in the Himalaya. *GSA Penrose Spec. Publ*. In press

Aristotle. c 340 B.C. *Meteorologica*. Transl. HDP Lee, 1987. Loeb Classical Library, ed. GP Goold. Cambridge, MA: Harvard Univ. Press. 432 pp.

Arkin PA, Xie P. 1994. The Global Precipitation Climatology Project: first algorithm intercomparison project. *Bull. Am. Meteorol. Soc.* 75:401–19

Bader MJ, Roach WT. 1977. Orographic rainfall in warm sectors of depressions. *Q. J. R. Meteorol. Soc.* 103:269–80

Baker MB. 1997. Cloud microphysics and climate. *Science* 276:1072–78

Banta RM. 1990. The role of mountain flows in making clouds. See Blumen 1990, pp. 229–83

Barros AP, Joshi M, Putkonen J, Burbank DW. 2000. A study of the 1999 monsoon rainfall in a mountainous region in central Nepal using TRMM products and rainguage observations. *Geophys. Res. Lett.* 27:3683–86

Barros AP, Lettenmaier DP. 1993. Dynamic modeling of the spatial distribution of precipitation in remote mountainous areas. *Mon. Weather Rev.* 121:1195–214

Barros AP, Lettenmaier DP. 1994a. Dynamic modeling of orographically induced precipitation. *Rev. Geophys.* 32:265–84

Barros AP, Lettenmaier DP. 1994b. Incorporation of an evaporative cooling scheme into a dynamic model of orographic precipitation. *Mon. Weather Rev.* 122:2777–83

Beaumont C, Fullsack P, Hamilton J. 1992. Erosional control of active compressional orogens. In *Thrust Tectonics*, ed. KR McClay, pp. 1–18. New York: Chapman & Hall

Bell TL, Kundu PN. 2000. Dependence of satellite sampling error on monthly averaged rain rates: comparison of simple models and recent studies. *J. Clim.* 13:449–62

Bergeron T. 1950. Über der mechanismus der ausgiebigan niederschläge. *Ber. Dtsch. Wetterd.* 12:225–32

Bergeron T. 1960. Operation and results of 'Project Pluvius'. In *Physics of Precipitation*, Monogr. 5, pp. 152–57. Washington, DC: Am. Geophys. Union

Bergeron T. 1961. Preliminary results of 'Project Pluvius'. *Publ. No. 53*, IASH, Comm. Land Eros, pp. 226–37

Bergeron T. 1968. *On the low-level distribution of atmospheric water caused by orography*. Presented at Int. Cloud Phys. Conf., Toronto

Blumen W, ed. 1990. *Atmospheric Processes Over Complex Terrain. Meteorol. Monogr.*, Vol. 23, No. 45. Boston, MA: Am. Meteorol. Soc.

Bolton D. 1980. The computation of equivalent potential temperature. *Mon. Weather Rev.* 108:1046–53

Bonacina LCW. 1945. Orographic rainfall and its place in the hydrology of the globe. *Q. J. R. Meteorol. Soc.* 71:41–55

Bougeault P, Binder P, Buzzi A, Dirks R, Houze RA, et al. 2001. The MAP special observing period. *Bull. Am. Meteorol. Soc.* 82:433–62

Bromwich DH. 1988. Snowfall in high southern latitudes. *Rev. Geophys.* 26:149–68

Browning KA, Hill FF, Pardoe CW. 1974. Structure and mechanism of precipitation and the effect of orography in a wintertime warm sector. *Q. J. R. Meteorol. Soc.* 100: 309–30

Bruintjes RT, Clark TL, Hall WD. 1994. Interactions between topographic airflow and cloud/precipitation development during the passage of a winter storm in Arizona. *J. Atmos. Sci.* 51:48–67

Caine N. 1980. The rainfall intensity: duration controls on shallow landslides and debris flows. *Geogr. Ann. Ser. A* 62:23–27

Caracena F, Maddox RA, Hoxit LR, Chappell CF. 1979. Mesoscale analysis of the Big Thompson storm. *Mon. Weather Rev.* 107:1–17

Carbone RE, Tuttle JD, Cooper WA, Grubišic V, Lee WC. 1998. Tradewind rainfall near the windward coast of Hawaii. *Mon. Weather Rev.* 126:2847–63

Carruthers DJ, Choularton TW. 1983. A model of the feeder-seeder mechanism of orographic rain including stratification and wind-drift effects. *Q. J. R. Meteorol. Soc.* 109:575–88

Chang ATC, Chiu LS, Wilheit TT. 1993a. Random erors of oceanic rainfall derived from SSM/I using probability distribution functions. *Mon. Weather Rev.* 121:2351–54

Chang ATC, Chiu LS, Wilheit TT. 1993b. Oceanic monthly rainfall derived from SSM/I. *EOS Trans. Am. Geophys. Union* 74(44):505–13

Chen C-S, Huang JM. 1999. A numerical study of precipitation characteristics over Taiwan Island during the winter season. *Meteorol. Atmos. Phys.* 70:167–83

Chen Q-S, Bromwich DH, Bai L. 1997. Precipitation over Greenland retrieved by a dynamic

method and its relation to cyclonic activity. *J. Clim.* 10:839–70

Choularton TW, Perry SJ. 1986. A model of the orographic enhancement of snowfall by the seeder-feeder mechanism. *Q. J. R. Meteorol. Soc.* 112:335–45

Colle BA. 2004. Sensitivity of orographic precipitation of changing ambient conditions and terrain geometries: an idealized modeling perspective. *J. Atmos. Sci.* 61:588–605

Colle BA, Westrick KJ, Mass CF. 1999. Evaluation of the MM5 and Eta-10 precipitation forecasts over the Pacific Northwest during the cool season. *Weather Forecast.* 14:137–54

Colton DE. 1976. Numerical simulation of the orographically induced precipitation distribution for use in hydrologic analysis. *J. Appl. Meteor.* 12:1241–51

Conway H, Raymond CF. 1993. Snow stability during rain. *J. Glaciol.* 39:635–42

Dai A, Wigley TML. 2000. Global patterns of ENSO-induced precipitation. *Geophys. Res. Lett.* 27:1283–86

Daly C, Neilson RP, Phillips DL. 1994. A statistical-topographic model for mapping climatological precipitation over mountainous terrain. *J. Appl. Meteorol.* 33:140–58

Douglas CKM, Glasspole J. 1947. Meteorological conditions in orographic rainfall in the British Isles. *Q. J. R. Meteorol. Soc.* 73:11–38

Doviak RJ, Zrnić DS. 1984. *Doppler Radar and Weather Observations*. Orlando, FL: Academic. 458 pp.

Durran DR. 1990. Mountain waves and downslope winds. See Blumen 1990, pp. 59–81

Durran DR. 2003. Lee waves and mountain waves. In *The Encyclopedia of the Atmospheric Sciences*, ed. J Holton, J Curry, J Pyle, pp. 1161–69. San Diego, CA: Academic

Durran DR, Klemp JB. 1982. The effects of moisture on trapped mountain lee waves. *J. Atmos. Sci.* 39:2490–506

Emanuel K. 1994. *Atmospheric Convection*. Oxford, UK: Oxford Univ. Press. 580 pp.

Evans JP, Smith RB, Oglesby R. 2003. Precipitation processes in the Middle East. *Proc. Int. Congr. Model. Simul., MODSIM03*, ed. D Post, Jupiters Hotel and Casino, Townsville, Aust., July 14–17

Ferretti R, Low-Nam S, Rotunno R. 2002. Numerical simulations of the Piedmont flood of 4–6 November, 1994. *Tellus A* 52:162–80

Fraser AB, Easter RC, Hobbs PV. 1973. A theoretical study of the flow of air and fallout of solid precipitation over mountainous terrain. Part I. Airflow model. *J. Atmos. Sci.* 30:801–12

Frei C, Schär C. 1998. A precipitation climatology of the Alps from high-resolution rain-gauge observations. *Int. J. Climatol.* 18:873–900

Geerts B, Heymsfield GM, Tian L, Halverson JB, Guillory A, Mejia MI. 2000. Hurricane Georges's landfall in the Dominican Republic: detailed airborne doppler radar imagery. *Bull. Am. Meteorol. Soc.* 81:999–1018

Grell GA, Dudhia J, Stauffer DR. 1995. A description of the fifth-generation Penn State NCAR Mesoscale Model (MM5). *NCAR Tech. Note TN-398 + STR.* 122 pp.

Griffiths GA, McSaveny MJ. 1983. Distribution of mean annual precipitation across some steepland regions of New Zealand. *NZ J. Sci.* 26:197–209

Groisman PY, Legates DR. 1994. The accuracy of United States precipitation data. *Bull. Am. Meteorol. Soc.* 75:215–27

Hill FF, Browning KA, Bader MJ. 1981. Radar and rain gauge observations of orographic rain over south Wales. *Q. J. R. Meteorol. Soc.* 107:643–70

Hobbs PV, Easter RC, Fraser AB. 1973. A theoretical study of the flow of air and fallout of solid precipitation over mountainous terrain. Part II. Microphysics. *J. Atmos. Sci.* 30:813–23

Hobbs PV, Matejka TJ, Herzegh PH, Locatelli JD, Houze RA. 1980. The mesoscale and microscale structure and organization of clouds and precipitation in midlatitude cyclones. I. A case study of a cold front. *J. Atmos. Sci.* 27:568–96

Houze RA. 1993. *Cloud Dynamics*. San Diego, CA: Academic. 570 pp.

Houze RA, James CN, Medina S. 2001. Radar observations of precipitation and airflow on the Mediterranean side of the Alps: Autumn 1998 and 1999. *Q. J. R. Meteorol. Soc.* 127: 2537–58

Iguchi T, Kozu T, Meneghini R, Awaka J, Okamoto K. 2000. Rain-profiling algorithm for the TRMM precipitation radar. *J. Appl. Meteorol.* 39:2038–52

IPCC. 2001. *Climate Change 2001: The Scientific Basis*, ed. JT Houghton, Y Ding, DJ Griggs, M Noguer, PJ van der Linden, et al. Cambridge, UK: Cambridge Univ. Press. 881 pp.

Jameson AR, Johnson DB. 1990. Cloud microphysics and radar. *Radar in Meteorology*, ed. D Atlas, pp. 322–40. Boston, MA: Am. Meteorol. Soc.

Jiang Q. 2003. Moist dynamics and orogaphic precipitation. *Tellus A* 55:301–16

Kageyama M, Valdes PJ, Ramstein G, Hewitt C, Wyputta U. 1999. Northern hemisphere storm tracks in present day and last glacial maximum climate simulations: a comparison of the European PMIP models. *J. Clim.* 12:742–60

Kalnay E, Kanamitsu M, Kistler R, Collins W, Deaven D, et al. 1996. The NCEP/NCAR 40-Year Reanalysis Project. *Bull. Am. Meteorol. Soc.* 77:437–71

Kapsner WR, Alley RB, Shuman CA, Anandakrishnan S, Grootes PM. 1995. Dominant influence of atmospheric circulation on snow accumulation in Greenland over the past 18,000 years. *Nature* 373:52–54

Katzfey JJ. 1995a. Simulation of extreme New Zealand precipitation events. Part I. Sensitivity of orography and resolution. *Mon. Weather Rev.* 123:737–54

Katzfey JJ. 1995b. Simulation of extreme New Zealand precipitation events. Part II. Mechanisms of precipitation development. *Mon. Weather Rev.* 123:755–75

Kawanishi T, Kuroiwa H, Kojima M, Oikawa K, Kozu T, et al. 2000. TRMM Precipitation Radar. *Adv. Space Res.* 25:969–72

Kidder SQ, Vonder Haar TH. 1995. *Satellite Meteorology: An Introduction*. San Diego, CA: Academic. 340 pp.

Kirshbaum DJ, Durran DR. 2004. Observations and modeling of banded orographic convection. *J. Atmos. Sci.* Submitted

Koutavas A, Lynch-Stieglitz J, Marchitto TM, Sachs JP. 2002. El Niño-like pattern in ice age tropical pacific sea surface temperature. *Science* 297:226–30

Krishnamurthy V, Shukla J. 2000. Intraseasonal and interannual variability of rainfall over India. *J. Clim.* 13:4366–77

Kummerow C, Simpson J, Thiele O, Barnes W, Chang ATC, et al. 2000. The status of the Tropical Rainfall Measuring Mission (TRMM) after two years in orbit. *J. Appl. Meteorol.* 39:1965–82

Lang JT, Barros AP. 2002. An investigation of the onsets of the 1999 and 2000 monsoons in central Nepal. *Mon. Weather Rev.* 130:1299–316

Lang JT, Barros AP. 2004. Winter storms in the central Himalayas. *J. Meteorol. Soc. Jpn.* 82:829–44

Levizzani V, Amorati R, Meneguzzo F. 2002. A review of satellite-based rainfall estimation methods. *Eur. Comm. Proj. MUSIC Rep.* (*EVK1-CT-2000-00058*). 66 pp.

Lin Y-L, Ensley DB, Chiao S, Huang C-Y. 2002. Orographic influence on rainfall and track deflection associated with the passage of a tropical cyclone. *Mon. Weather Rev.* 130:2929–50

Mass CF. 1981. Topographically-forced convergence in western Washington State. *Mon. Weather Rev.* 109:1335–47

McCauley MP, Sturman AP. 1999. A study of orographic blocking and barrier wind development upstream of the Southern Alps, New Zealand. *Meteorol. Atmos. Phys.* 70:121–31

Medina S, Houze RA. 2003. Air motions and precipitation growth in alpine storms. *Q. J. R. Meteorol. Soc.* 129:345–71

Middleton WEK. 1966. *A History of the Theories of Rain*. New York: Franklin-Watts. 223 pp.

Miller A. 1976. The climate of Chile. In *Climates of Central and South America. World Survey of Climatology*, ed. W Schwerdtfeger, pp. 113–45. Amsterdam: Elsevier

Montgomery DR, Balco G, Willett SD. 2001. Climate, tectonics, and the morphology of the Andes. *Geology* 29:579–82

Myers VA. 1962. Airflow on the windward side of the ridge. *J. Geophys. Res.* 67:4267–91

Noren AJ, Bierman PR, Steig EJ, Lini A, Southon J. 2002. Millennial-scale storminess variability in the northeastern United States during the Holocene epoch. *Nature* 419:821–24

Ohmura A, Reeh N. 1991. New precipitation and accumulation maps for Greenland. *J. Glaciol*. 43:140–45

Peixoto JP, Oort AH. 1992. *Physics of Climate*. New York: Am. Inst. Phys. 520 pp.

Rasmusson EM, Arkin PA. 1993. A global view of large scale precipitation variability. *J. Clim.* 6:1495–522

Ray PS. 1990. Convective dynamics. In *Radar Meteorology*, ed. D Atlas, pp. 348–90. Boston, MA: Am. Meteorol. Soc.

Reiners PW, Ehlers TA, Mitchell SG, Montgomery DR. 2003. Coupled spatial variations in precipitation and long-term erosion rates across the Washington Cascades. *Nature* 426:645–47

Rhea JO. 1978. Orographic precipitation model for hydrometeorological use. *Colorado State Univ. Atmos. Pap. 287*. 198 pp.

Robichaud AJ, Austin GL. 1988. On the modeling of warm orographic rain by the seeder-feeder mechanism. *Q. J. R. Meteorol. Soc.* 114:967–88

Roe GH. 2002. Modeling precipitation over ice sheets: an assessment using Greenland. *J. Glaciol.* 48:70–80

Roe GH, Baker MB. 2004. Controls on the pattern of orographic precipitation. *J. Atmos. Sci.* Submitted

Roe GH, Lindzen RS. 2001. The mutual interaction between continental-scale ice sheets and atmospheric stationary waves. *J. Clim.* 14:1450–65

Roe GH, Stolar DR, Willett SD. 2004. Response of a steady-state critical orogen to changes in climatic and tectonic forcing. *GSA Penrose Spec. Publ*. In press

Rotunno R, Ferretti R. 2001. Mechanisms of intense alpine rainfall. *J. Atmos. Sci.* 58:1732–49

Rupper S, Steig EJ, Roe GH. 2004. On the relationship between snow accumulation at Mt. Logan, Yukon, and climate variability in the North Pacific. *J. Clim.* 17:4724–39

Sanberg JAM, Oerlemans J. 1983. Modeling of Pleistocene European ice sheets: the effect of upslope precipitation. *Geol. Mijnb.* 62:267–73

Sarker RP. 1966. A dynamical model of orographic rainfall. *Mon. Weather Rev.* 94:555–72

Sawyer JS. 1956. The physical and dynamical problems of orographic rain. *Weather* 11:375–81

Shin K, North GR. 1988. Sampling error study for rainfall estimate by satellite using a stochastic model. *J. Appl. Meteorol.* 27:1218–31

Simmons AJ, Gibson JK. 2000. *The ERA-40 Proj. Plan, ERA-40 Proj. Rep. Ser. No. 1*. Reading, UK: ECMWF. 63 pp.

Simpson J, Adler RE, North GR. 1988. A proposed tropical rainfall measuring mission (TRMM) satellite. *Bull. Am. Meteorol. Soc.* 69:278–95

Sinclair MR. 1994. A diagnostic model for estimating orographic precipitation. *J. Appl. Meteorol.* 33:1163–75

Sinclair MR, Wratt DS, Henderson RD, Gray WR. 1997. Factors affecting the distribution and spillover of precipitation in the Southern Alps of New Zealand—a case study. *J. Appl. Meteorol.* 36:428–42

Smith RB. 1979. The influence of mountains on the atmosphere. *Adv. Geophys.* 21:87–230

Smith RB. 2003. A linear uplsope-time delay model for orographic precipitation. *J. Hydrol.* 282:2–9

Smith RB. 2004. Progress on the theory of orographic precipitation. *GSA Penrose Spec. Publ*. In press

Smith RB, Barstad I. 2004. A linear theory of orographic precipitation. *J. Atmos. Sci.* 61: 1377–91

Smith RB, Jiang Q, Fearon MG, Tabary P, Dorninger M, et al. 2003. Orographic precipitation and air mass transformation: an Alpine example. *Q. J. R. Meteorol. Soc.* 129: 433–54

Spencer RW. 1993. Global oceanic precipitation from the MSU during 1979–91 and comparison to other climatologies. *J. Clim.* 6:1301–26

Steiner M, Bousquet O, Houze RA, Smull BF, Mancini M. 2003. Airflow within major Alpine river valleys under heavy rainfall. *Q. J. R. Meteorol. Soc.* 129:411–31

Stow FW. 1875. The rainfall of 1875 in Wensleydale and district. *Symons's Br. Rainfall, 1875*, pp. 10–20

Thompson DWJ, Wallace JM. 2001. Regional climate impacts of the Northern Hemisphere annular mode. *Science* 293:85–89

Wallace JM, Hobbs PV. 1977. *Atmospheric Science: An Introductory Survey*. San Diego, CA: Academic. 465 pp.

Wang YG, Cheng H, Edwards RL, An Z-S, Wu JY, et al. 2001. A high-resolution absolute-dated late Pleistocene monsoon record from Hulu Cave, China. *Science* 294:2345–48

Willett SD. 1999. Orogeny and orography: The effects of erosion on the structure of mountain belts. *J. Geophys. Res.* 104:28957–81

Wratt DS, Revell MJ, Sinclair MR, Gray WR, Henderson RD, Chater AM. 2000. Relationships between air mass properties and mesoscale rainfall in New Zealand's Southern Alps. *Atmos. Res.* 52:261–82

Wratt DS, Ridley RN, Sinclair MR, Larsen H, Thompson SM, et al. 1996. The New Zealand Southern Alps experiment. *Bull. Am. Meteorol. Soc.* 77:683–92

Xie P, Arkin PA. 1997. Global precipitation: A 17-year monthly analysis based on gauge observations, satellite estimates, and numerical model outputs. *Bull. Am. Meteorol. Soc.* 78:2539–58

Yuter SA, Houze RA. 2003. Microphysical modes of precipitation growth determined by S-band vertically pointing radar in orographic precipitation during MAP. *Q. J. R. Meteorol. Soc.* 129:455–76

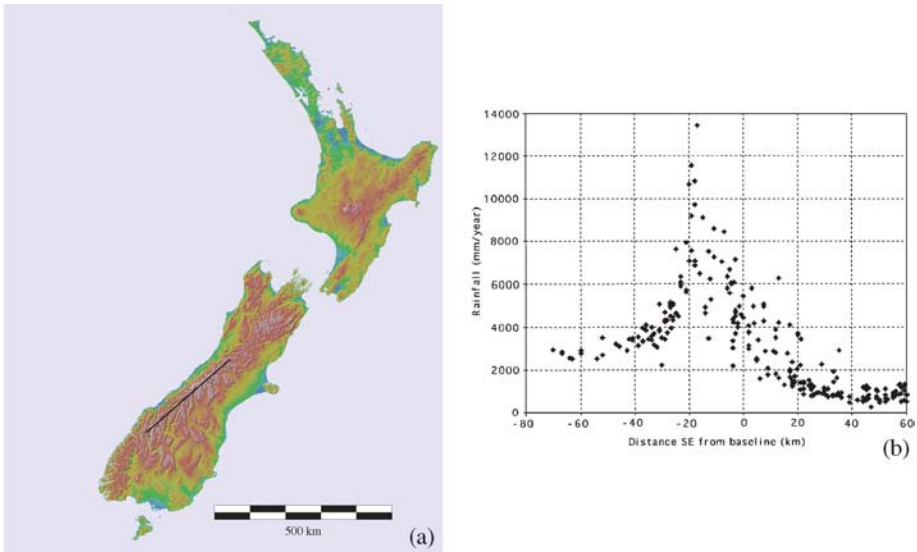

Figure 1 (*a*) Orography of New Zealand. (*b*) Precipitation gauge measurements of annual precipitation rates over the Southern Alps rates as a function of distance from the average crest line, indicated with a line in (*a*). From Wratt et al. (2000). Reproduced by permission of Elsevier.

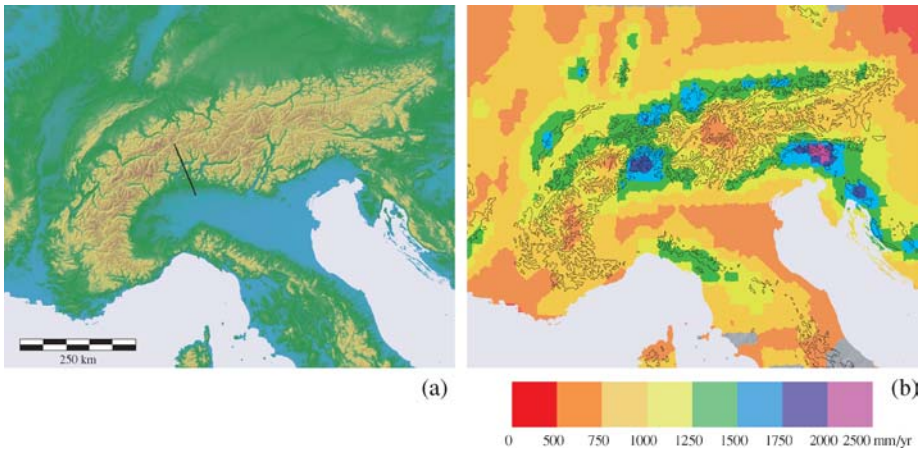

Figure 2 (*a*) Orography of the European Alps. The straight black line in the Laggo Maggiore region shows the transect for the radar profile in Figure 4*b*. (b) Annual precipitation rate, interpolated by Frei & Schär (1998) from precipitation gauge measurements for the years 1971–1990. Elevation contours at 1000 m and 2000 m are also shown.

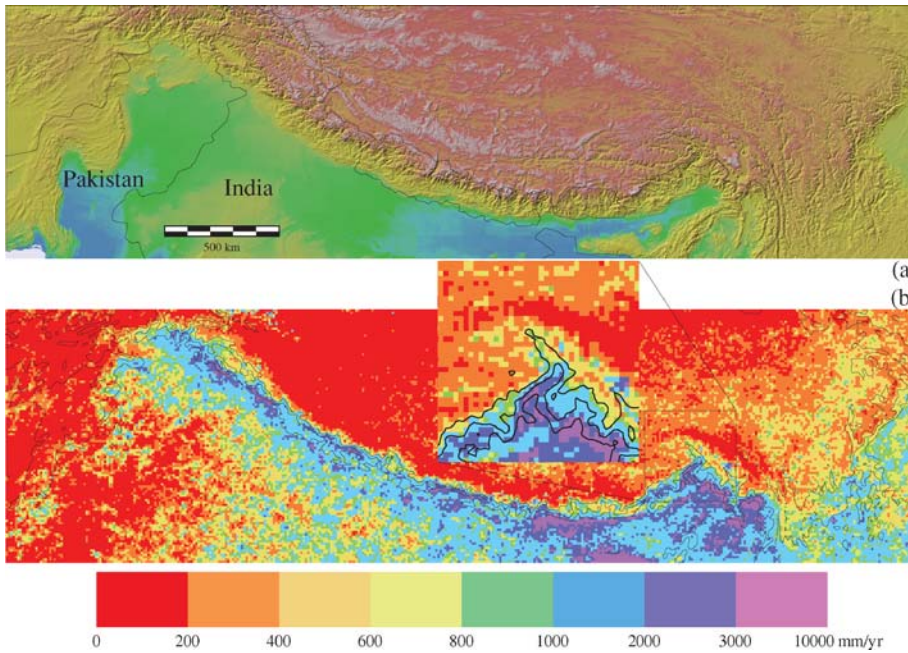

Figure 3 (*a*) Orography of the Tibetan Plateau. (*b*) Annual precipitation total estimated from the TRMM satellite (from Anders et al. 2004c). Elevation contours at 1500 m, 2500 m, and 3500 m are also shown. The inset shows an expanded view of the region around Namche Barwa.

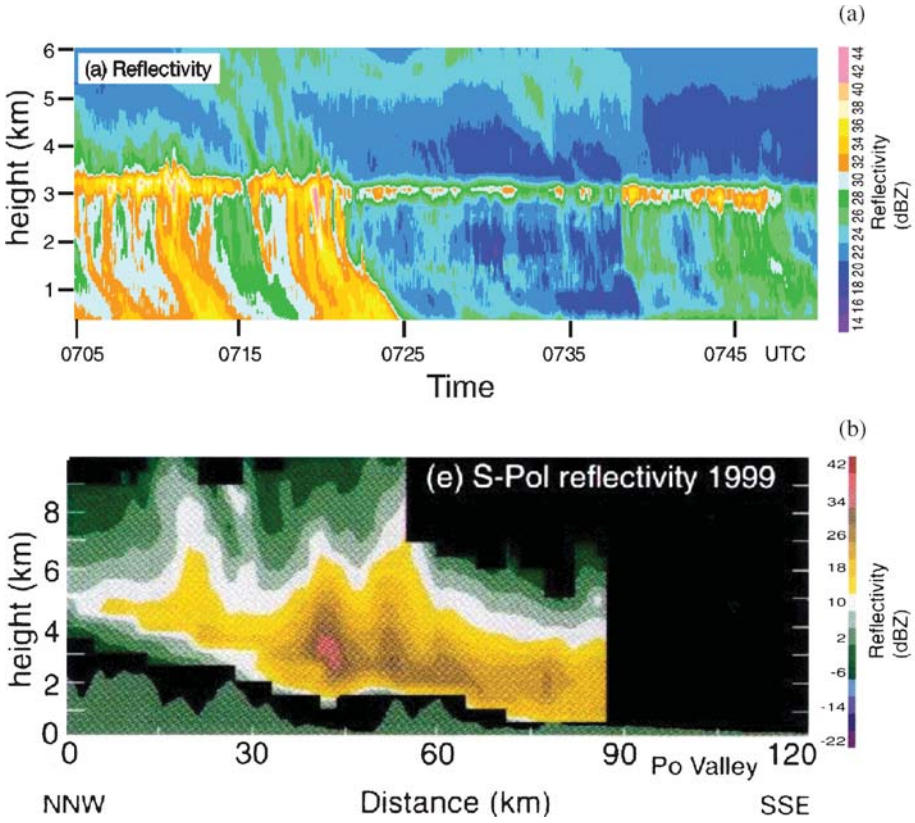

Figure 4 (*a*) 45-min time series of reflectivity during a storm (September 20, 1999) from a vertically pointed radar at Locarno-Monti, Switzerland (adapted from Yuter & Houze 2003). The melting layer shows as a bright band at approximately 3 km. Note the rapid fluctuations in reflectivity; (*b*) mean radar reflectivity as a function of height and distance along the transect shown in Figure 2*a*, from September to November, 1999 (adapted from Houze et al. 2001). The localized reflectivity maxima in (*b*) reflect convection occurring within stratiform precipitation. Reproduced by permission of the Royal Meteorological Society.

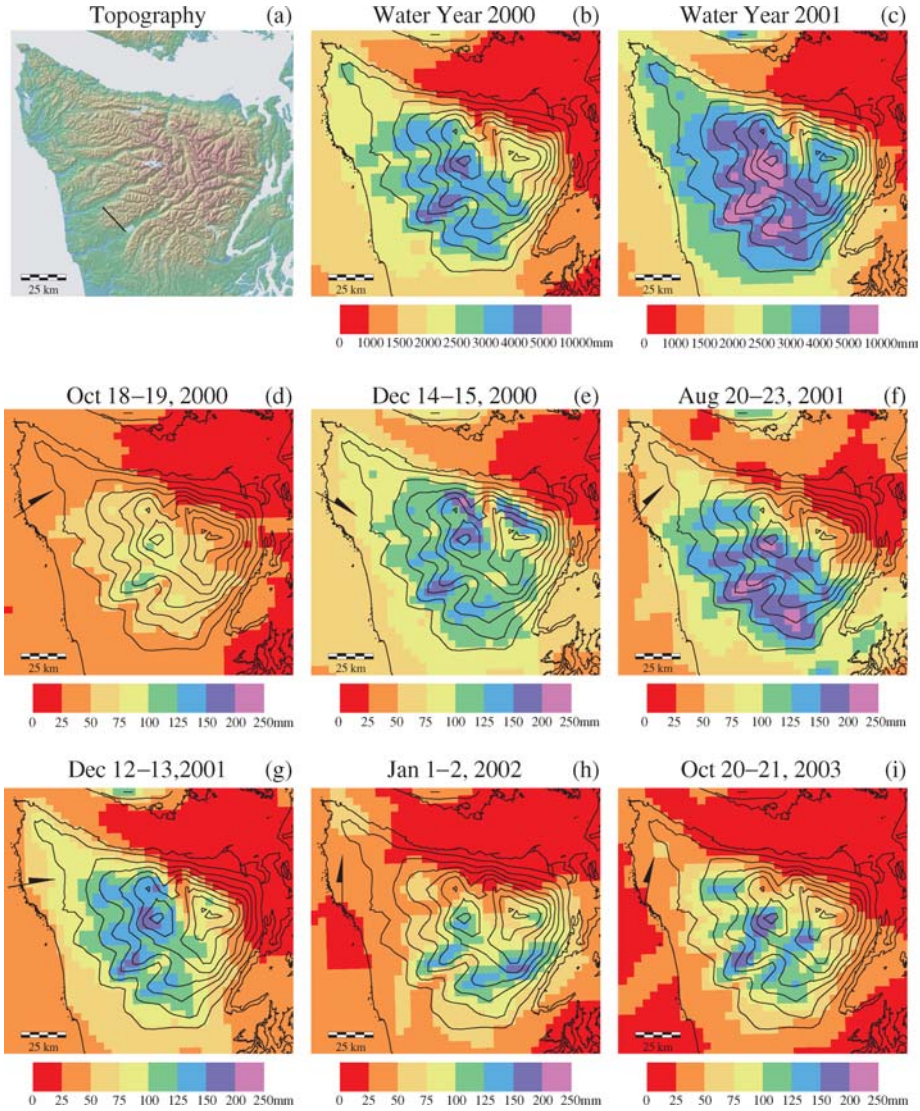

Figure 8 (*a*) Orography of the Olympic mountains in Washington State. (*b*,*c*) MM5 output for total precipitation in the 2000 and 2001 water years (the 2000 water year is October 2000 to September 2001). Note the 40% difference in annual totals and the presence of a dry slot in the lee of Mt. Olympus. (*d–i*) precipitation totals in the MM5 output from various storms. The arrows centered on Quillayute indicate the direction of the average wind in the 800 to 600 mb layer, measured by the Quillayute radiosonde launch at the time closest to the maximum precipitation rate in the storm. The basic precipitation pattern persists despite different wind directions and precipitation totals. The MM5 model was run at 4 km resolution. Height contours of the MM5 model orography are plotted every 200 m. The black line in panel (*a*) gives the transect of precipitation gauges shown in Figure 9.

Annual Review of Earth and Planetary Sciences
Volume 33, 2005

CONTENTS